

Measuring the Hubble constant through the galaxy pairwise peculiar velocity

WANGZHENG ZHANG ¹, MING-CHUNG CHU ¹, SHIHONG LIAO ², SHEK YEUNG,¹ AND HUI-JIE HU ^{3,2}

¹*Department of Physics, the Chinese University of Hong Kong, Sha Tin, NT, Hong Kong*

²*Key Laboratory for Computational Astrophysics, National Astronomical Observatories, Chinese Academy of Sciences, Beijing 100101, China*

³*University of Chinese Academy of Sciences, No. 19 A Yuquan Road, Beijing 100049, China*

ABSTRACT

The Hubble constant H_0 , the current expansion rate of the universe, is one of the most important parameters in cosmology. The cosmic expansion regulates the mutually approaching motion of a pair of celestial objects due to their gravity. Therefore, the mean pairwise peculiar velocity of celestial objects, which quantifies their relative motion, is sensitive to both H_0 and the dimensionless total matter density Ω_m . Based on this, using the Cosmicflows-4 data, we measured H_0 for the first time via the galaxy pairwise velocity in the nonlinear and quasi-linear range. Our results yield $H_0 = 75.5 \pm 1.4 \text{ km s}^{-1} \text{ Mpc}^{-1}$ and $\Omega_m = 0.311^{+0.029}_{-0.028}$. The uncertainties of H_0 and Ω_m can be improved to around 0.6% and 2%, respectively, if the statistical errors become negligible in the future.

Keywords: Cosmological parameters (339); Hubble constant (758); N-body simulations (1083)

1. INTRODUCTION

Although the Lambda Cold Dark Matter (Λ CDM) model achieves great success in describing a wide range of cosmological observations, the Hubble tension, i.e., the significant difference in the values of the Hubble constant H_0 between indirect and direct measurements, suggests that physics beyond Λ CDM may be needed. Specifically, the H_0 determined by the anisotropies of cosmic microwave background (CMB) from Planck ($H_0 = 67.36 \pm 0.54 \text{ km s}^{-1} \text{ Mpc}^{-1}$, Planck Collaboration et al. 2020) deviates by almost 5σ from that measured using Type Ia supernovae (SNeIa) calibrated by Cepheids (SH0ES, $H_0 = 73.04 \pm 1.04 \text{ km s}^{-1} \text{ Mpc}^{-1}$, Riess et al. 2022). More details can be found, for example, in Abdalla et al. (2022); Schöneberg et al. (2022); Perivolaropoulos & Skara (2022). Other independent CMB measurements, such as ACT (Choi et al. 2020) and SPT-3G (SPT-3G Collaboration et al. 2023), give consistent results on H_0 as Planck's. H_0 can also be measured using different distance ladder calibrators other than Cepheids, such as the tip of the red-giant branch (TRGB, Freedman 2021; Anand et al. 2022), surface brightness fluctuations (SBF) of galaxies (Khetan et al. 2021; Blakeslee et al. 2021), Miras variables (Huang et al. 2020), or the Tully-Fisher relation (TFR, Kourkchi et al. 2020; Schombert et al. 2020). Furthermore, H_0

can be obtained from other independent measurements that do not rely on the distance ladder, such as through Masers (Pesce et al. 2020), gravitational lensing (Wong et al. 2020; Birrer et al. 2020), gravitational waves (Gayathri et al. 2021; The Ligo Scientific Collaboration et al. 2023), or cosmic chronometers (Moresco et al. 2022). Although not all of the direct measurements of H_0 are in tension with indirect measurements, most are significantly larger than the latter, particularly Planck's.

Therefore, more independent ways to measure H_0 are desirable. In this Letter, we measure H_0 using galaxy velocity statistics in the nonlinear and quasi-linear regime for the first time. Typically, H_0 is derived by balancing the overall infall and outflow of galaxies (Tully et al. 2016, 2023). Here, we extend this by considering the relative motion of galaxies, i.e., through the mean pairwise peculiar velocity $v_{12}(r)$, also known as pairwise velocity, which is defined as

$$v_{12}(r) \equiv \langle [\mathbf{v}_1(\mathbf{r}_1) - \mathbf{v}_2(\mathbf{r}_2)] \cdot \hat{\mathbf{r}} \rangle, \quad (1)$$

where $\mathbf{r} \equiv \mathbf{r}_1 - \mathbf{r}_2$ is the distance vector between a pair of objects such as galaxies or halos in the comoving frame with peculiar velocities $\mathbf{v}_{1/2}$. The average $\langle \dots \rangle$ is taken over all pairs with separation $r \equiv |\mathbf{r}|$, and $v_{12}(r)$ depends only on r according to isotropy. The pairwise velocity quantifies the relative motion of pairs of objects with separation r . For objects with a conserved number, we have

$$\frac{v_{12}(r, a)}{Hra} = -\frac{a}{3[1 + \Xi(r, a)]} \frac{\partial \Xi(r, a)}{\partial a}, \quad (2)$$

where $\bar{\Xi}(r, a) \equiv (3/4\pi r^3) \int_0^r d^3\mathbf{y} \Xi(y, a)$ and Ξ is the two-point correlation function. $H = \dot{a}/a$ is the Hubble parameter and a is the scale factor (Mo et al. 2010, §6; Peebles 2020, §71). Therefore, the pairwise velocity contains information on how the two-point correlation evolves. At $r \lesssim 0.2$ Mpc, due to the stable clustering, $v_{12}(r, a) = -Hra$ (Mo et al. 2010, §6). At $r \gtrsim 30$ Mpc, under the linear approximation, $v_{12}(r, a) = -2Hra f \bar{\Xi}(r, a)/3[1 + \Xi(r, a)]$ (Juszkiewicz et al. 1999), where the linear growth rate $f \equiv d \ln D / d \ln a \approx \Omega_m^{0.55}$ (Linder 2005). D and Ω_m are the linear growth solution and dimensionless total matter density, respectively. Consequently, $v_{12}(r)$ is sensitive to H_0 and Ω_m . In this Letter, we focus on the nonlinear and quasi-linear range $r \leq 16$ Mpc, which requires N-body simulations for accurate predictions and cannot be adequately described by the linear perturbation theory (Kosowsky & Bhattacharya 2009; Bhattacharya et al. 2011; Mueller et al. 2015a,b; Jaber et al. 2024). There are at least two advantages using $v_{12}(r)$ to measure H_0 from the observational point of view. Firstly, any object with a known peculiar velocity can be used in the measurement. Secondly, any common systematic errors of the measured peculiar velocities, e.g., the peculiar motion of the Milky Way, would be largely cancelled in the pairwise velocity.

The pairwise velocity and its related quantities have been well studied to constrain cosmological parameters such as σ_8 and Ω_m (Juszkiewicz et al. 2000; Feldman et al. 2003; Ma et al. 2015), the local growth rate $f\sigma_8$ (Howlett et al. 2017; Dupuy et al. 2019), dark energy or modified gravity models (Bhattacharya & Kosowsky 2008; Bhattacharya et al. 2011; Mueller et al. 2015a; Bibiano & Croton 2017; Jaber et al. 2024), and the kinematic Sunyaev-Zeldovich (kSZ) effect (Bhattacharya & Kosowsky 2007; Calafut et al. 2021), which is also used to constrain neutrino masses (Mueller et al. 2015b).

The remainder of this Letter is organized as follows. In Sections 2 and 3, we discuss how $v_{12}(r)$ is calculated in N-body simulations and observations, respectively. The fitting method and results are elaborated in Section 4. In Section 5, we present the summary and discussions.

2. HALO-HALO PAIRWISE VELOCITY

We perform our cosmological N-body simulations using a modified grid-based neutrino-involved `Gadget-2` (Springel 2005; Zhang et al. 2024) with three types of neutrinos with a degenerate mass of 0.02 eV. We sample the Hubble constant $H_0 = 67.6, 70.6, 73.6, 76.6,$ and $79.6 \text{ km s}^{-1} \text{ Mpc}^{-1}$ and $\Omega_m = 0.274, 0.304,$ and 0.334 . The scalar index $n_s = 0.9652$ and the corresponding spectral amplitude $A_s = 2.0968 \times 10^{-9}$ are from the Planck CMB results (Planck Collaboration et al. 2020). The baryon density $\Omega_b h^2 = 0.02244$ is from the big bang nucleosynthesis results (Navas et al. 2024). The initial conditions of the simulations are generated by `2LPTic` (Crocce et al. 2006), and the initial power spectra at redshift $z = 99$ are obtained by `CAMB` (Lewis et al. 2000).

We run dark-matter-only (DMO) simulations with the number of dark matter particles $N_p = 1024^3$ and box size $L_{\text{box}} = 250 h^{-1} \text{ Mpc}$ ($h \equiv H_0/100$ is the dimensionless Hubble constant). For the set $H_0 = 73.6 \text{ km s}^{-1} \text{ Mpc}^{-1}$ and $\Omega_m = 0.334$, we set up three runs, which differ only by the initial random seeds. Each run comprises four separate simulations (normal, paired, fixed, paired and fixed), i.e., a total of 12 simulations, to reduce the impact of cosmic variance (Angulo & Pontzen 2016; Klypin et al. 2020).

The dark matter halos are found by `ROCKSTAR` (Behroozi et al. 2013). This Letter adopts halo masses as per Bryan & Norman (1998). The center and velocity of the halo are determined by averaging the positions of dark matter particles in the inner subgroup and the velocities of dark matter particles within the innermost 10% of the halo’s virial radius, respectively (Behroozi et al. 2013). Hereafter, we only consider host halos with at least 200 dark matter particles. The mean halo-halo pairwise peculiar velocity $v_{\text{hh}}(r)$ is calculated via Eq. (1). To consistently compare with observations, we convert the default unit $h^{-1} \text{ Mpc}$ in each simulation to Mpc using the corresponding h .

3. GALAXY-GALAXY PAIRWISE VELOCITY

In this Letter, we use the grouped catalog from Cosmicflows-4 (CF-4, Tully et al. 2023), which minimizes distance uncertainties through weighted averaging of galaxy members. Although our analysis is based on the grouped catalog, we have confirmed that using the brightest galaxies in the ungrouped catalog produces consistent results. The farthest galaxy used in this Letter is at redshift around 0.1. Hence, we compare the data with only the redshift-0 halos from simulations. As shown in Zhang et al. (2024), the magnitude and shape of $v_{\text{hh}}(r)$ are sensitive to the range of halo virial masses used in the calculation. To consistently compare the data with our simulation results, we need to match their halo mass ranges. Therefore, next, we will discuss how we extract the halo mass information from the CF-4 grouped catalog, followed by the galaxy-galaxy pairwise velocity $v_{\text{gg}}(r)$ calculation along with its error estimation.

3.1. Mass information

We obtain the stellar masses of the CF-4 galaxies through the light-to-stellar-mass relation (Bell et al. 2003),

$$\log_{10} \left(\frac{M_g/M_\odot}{L_\lambda/L_{\odot\lambda}} \right) = a_\lambda + b_\lambda \times (B - V), \quad (3)$$

where λ denotes the different observational bands, and M_g is the galaxy stellar mass. L_λ is the luminosity for the λ band, and $B - V$ is the difference between the apparent magnitudes in the B and V bands of the galaxy. The coefficients a_λ and b_λ are taken from Table 7 of Bell

et al. (2003). Specifically, we use B and I bands, i.e., $a_B = -0.942$, $b_B = 1.737$ and $a_I = -0.399$, $b_I = 0.824$ ¹. The corresponding B and I band luminosities are obtained by

$$2.5 \log_{10} \left(\frac{L_{B(I)}}{L_{\odot B(I)}} \right) = M_{\odot B(I)} - m_{B(I)} + \mu_g, \quad (4)$$

where the B and I band apparent magnitudes $m_{B(I)}$ and distance moduli μ_g are taken from HyperLeda (Makarov et al. 2014) after matching with the Principal Galaxies Catalog (PGC) identification. The absolute magnitude of the Sun in the $B(I)$ band is $M_{\odot B(I)} = 5.44$ (4.10) (Willmer 2018).

Then, we can infer the virial masses of the corresponding host halos M_h from the stellar-to-halo-mass relation (Moster et al. 2010),

$$\frac{M_g}{M_h} = 2C_0 \left[\left(\frac{M_h}{M_{h1}} \right)^{-\beta} + \left(\frac{M_h}{M_{h1}} \right)^{\gamma} \right]^{-1}, \quad (5)$$

where $C_0 = 0.02817$, $\beta = 1.068$, $\gamma = 0.611$ and $M_{h1} = 10^{11.899} M_{\odot}$.

For each galaxy in the CF-4 grouped catalog, we identify its members using the CF-4 ungrouped catalog and compute the total stellar mass via Eq. (3), which is then used to estimate the host halo virial mass via Eq. (5). We find that most of the corresponding host halo virial masses are within the range $[10^{11}, 10^{13}] M_{\odot}$. Therefore, we select galaxies and simulation host halos that have host halo virial masses within the range $[10^{11}, 10^{13}] M_{\odot}$, obtaining a total of around 30,000 galaxies and 200,000 simulation host halos.

3.2. Peculiar velocity

Following Davis & Scrimgeour (2014); Ma et al. (2015), the line-of-sight peculiar velocity v_p of a certain galaxy is calculated by

$$v_p = \frac{f(\bar{z})V_{\text{cmb}} - H_0 D_L}{f(\bar{z}) + H_0 D_L/c}, \quad (6)$$

where c is the speed of light. The systemic velocity of the galaxy in the CMB rest frame V_{cmb} and its luminosity distance D_L are from the CF-4 grouped catalog (Tully et al. 2023), while $f(\bar{z})$ can be calculated assuming flat Λ CDM by

$$f(\bar{z}) = 1 + \frac{1}{2}[1 - q_0]\bar{z} - \frac{1}{6}[2 - q_0 - 3q_0^2]\bar{z}^2, \quad (7)$$

where $q_0 = (3\Omega_m - 2)/2$. Given Ω_m and H_0 , the cosmological redshift \bar{z} is calculated from

$$D_L(\bar{z}) = (1 + \bar{z}) \int_0^{\bar{z}} \frac{cdz'}{H(z')}, \quad (8)$$

¹ In calculation, we subtract a_{λ} by 0.15 dex for the Kroupa initial mass function (IMF) as suggested in Bell et al. (2003).

where $H(z) = H_0 \sqrt{\Omega_m(1+z)^3 + 1 - \Omega_m}$.

Due to the uncertainties of the distances, the peculiar velocities calculated from Eq. (6) can reach 10,000 km s⁻¹ for some galaxies. To exclude these extreme cases, we calculate the line-of-sight velocities of host halos with comparable masses ($[10^{11}, 10^{13}] M_{\odot}$) in the Uchuu simulations (Ishiyama et al. 2021). By placing observers at random locations within the simulation box, we generate three mock samples of host halo line-of-sight velocities, all of which follow perfect Gaussian distributions with $3\sigma \approx 1000$ km s⁻¹. Therefore, we only consider galaxies satisfying $|v_p| \leq v_p^{\text{max}}$, with $v_p^{\text{max}} = 1000$ km s⁻¹, leaving us with 10,014 galaxies. More details can be found in Appendix A.

3.3. Position

The comoving position of each galaxy is calculated by

$$\begin{aligned} x &= D_c \cos \delta \cos \alpha, \\ y &= D_c \cos \delta \sin \alpha, \\ z &= D_c \sin \delta, \end{aligned} \quad (9)$$

where the right ascension J2000 α and declination J2000 δ of each galaxy are from the CF-4 grouped catalog (Tully et al. 2023), and the comoving distance $D_c \equiv D_L/(1 + \bar{z})$.

3.4. Galaxy-galaxy pairwise velocity

As we can only observe the line-of-sight peculiar velocity, we calculate the galaxy-galaxy pairwise velocity by the following estimator (Ferreira et al. 1999),

$$v_{\text{gg}}(r) = \frac{\sum_{A,B} (v_{p,A} - v_{p,B}) p_{AB}}{\sum_{A,B} p_{AB}^2}, \quad (10)$$

where $v_{p,A/B}$ is the line-of-sight peculiar velocity of galaxy A/B calculated using Eq. (6), and $p_{AB} \equiv \hat{\mathbf{r}} \cdot (\hat{\mathbf{r}}_A + \hat{\mathbf{r}}_B)/2$, with $\mathbf{r} = \mathbf{r}_A - \mathbf{r}_B$. The comoving positions of galaxies are denoted as $\mathbf{r}_{A/B}$ and calculated using Eq. (9). The summation is over all galaxy pairs with separation equal to r .

Based on Eq. (10), we explore how the variation of v_p^{max} (from 1000 km s⁻¹ to 800 and 1200 km s⁻¹) impacts v_{gg} and find that only for $r \lesssim 16$ Mpc, v_{gg} is not sensitive to the choice of v_p^{max} . Consequently, we calculate v_{hh} and v_{gg} in the range $r \in [0, 16]$ Mpc using 8 linear bins. More details are provided in Appendix A.

3.5. Observational error sources

In this section, we present the error sources in galaxy-galaxy pairwise velocity v_{gg} , as shown in Figure 1. All calculations in the following are based on $H_0 = 74.6$ km s⁻¹ Mpc⁻¹ and $\Omega_m = 0.27$ suggested by CF-4 (Tully et al. 2023).

3.5.1. Jackknife

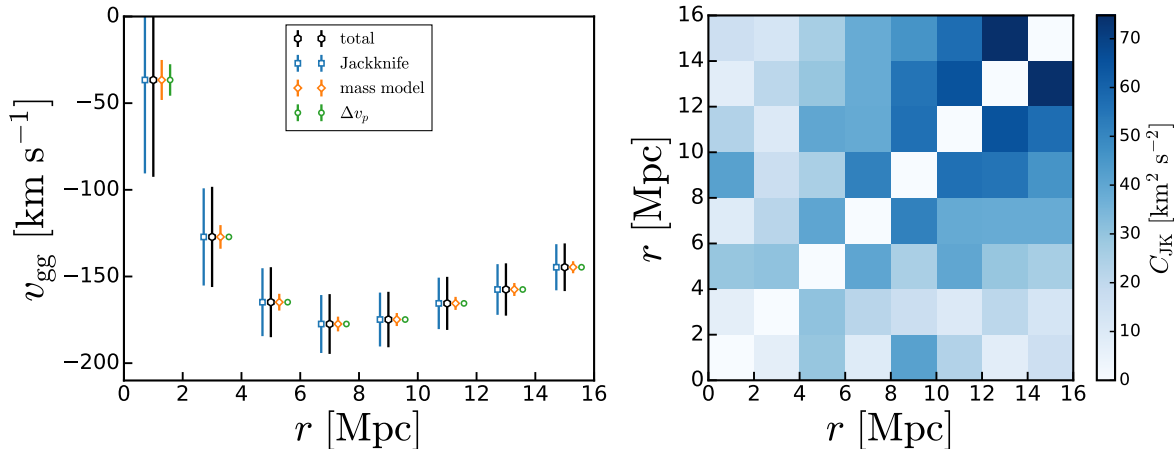


Figure 1. Error sources of v_{gg} and the same r bins in different colored symbols are shifted horizontally slightly for clarity (left panel). The Covariance matrix of C_{JK} for different r bins, with diagonal terms manually set to be 0 (right panel), where the colors show the magnitudes of C_{JK} .

We use Jackknife by `Astropy` (Astropy Collaboration et al. 2013, 2018, 2022) to estimate the statistical covariance matrix of v_{gg} , denoted as C_{JK} ,

$$[C_{\text{JK}}]_{ij} = \frac{N_{\text{gr}} - 1}{N_{\text{gr}}} \sum_{k=1}^{N_{\text{gr}}} \left[v_{\text{gg}}^{(k)}(r_i) - \bar{v}_{\text{gg}}^{\text{jack}}(r_j) \right]^2, \quad (11)$$

where $N_{\text{gr}} = 10,014$ is the number of galaxies and $\bar{v}_{\text{gg}}^{\text{jack}}(r) \equiv \sum_{k=1}^{N_{\text{gr}}} v_{\text{gg}}^{(k)}(r) / N_{\text{gr}}$. The term $v_{\text{gg}}^{(k)}$ is derived from the k^{th} Jackknife sub-sample, incorporating all galaxies except the k^{th} one. The errors from the diagonal terms of C_{JK} are shown as blue squares in the left panel of Figure 1, while the off-diagonal terms are shown in the right panel.

3.5.2. Peculiar velocity error

When the line-of-sight peculiar velocity v_p of a galaxy is calculated from Eq. (6), we transfer the luminosity distance error ΔD_L on it (from the CF-4 grouped catalog (Tully et al. 2023)), denoted as Δv_p , and this is transferred to the final v_{gg} , denoted as σ_{v_p} . This error is reduced due to the relatively large number of pairs, especially in the large r bins, shown as green circles in the left panel of Figure 1.

3.5.3. Mass model

In our pipeline, we first use Eqs. (3) and (5) to determine the corresponding halo mass of a galaxy; then, we choose galaxies with halo masses within $[10^{11}, 10^{13}] M_{\odot}$ to calculate v_{gg} .

Hence, here we consider the possible uncertainty caused by this procedure. First, $\log_{10}(M_g)$ in Eq. (3) has around 0.1 dex scatter (Bell et al. 2003), and also the coefficients in Eq. (5) have errors, i.e., $\Delta C_0 = 0.0006$, $\Delta(\log_{10} M_1) = 0.025$, $\Delta\beta = 0.0475$, and $\Delta\gamma = 0.011$

² (Moster et al. 2010). All of these can be propagated to the uncertainty of the final computed halo mass $\log_{10} M_h$, denoted as $\Delta(\log_{10} M_h)$.

Then we apply resampling 10,000 times. In each resampling, we generate a halo mass according to the Gaussian distribution centered at $\log_{10} M_h$ with width $\Delta(\log_{10} M_h)$, and we choose galaxies with halo masses within $[10^{11}, 10^{13}] M_{\odot}$ to recalculate v_{gg} accordingly.

Finally, we take the one sigma scatter of such resamplings, denoted as σ_{mass} , to characterize the uncertainty of mass models we used, shown as orange diamond error bars in the left panel of Figure 1.

3.5.4. Total error

The total covariance matrix of v_{gg} , denoted as C_{gg} , combines contributions from all three sources discussed above, i.e., $[C_{\text{gg}}]_{ij} = [C_{\text{JK}}]_{ij} + (\sigma_{v_p})^2 \delta_{ij} + (\sigma_{\text{mass}})^2 \delta_{ij}$. The diagonal terms are shown as black hexagonal error bars in the left panel of Figure 1, which are mainly due to Jackknife.

In this section, although H_0 is set to $74.6 \text{ km s}^{-1} \text{ Mpc}^{-1}$ and Ω_m to 0.27, σ_{mass} is independent of H_0 and Ω_m . In the following analysis, σ_{v_p} is recalculated for various H_0 and Ω_m , assuming that C_{JK} does not change across these combinations.

4. RESULTS

As discussed in Section 3.4, hereafter, the galaxy-galaxy pairwise velocity (v_{gg}) and halo-halo pairwise velocity (v_{hh}) are calculated over $r \in [0, 16]$ Mpc using 8 linear bins.

The effects of H_0 and Ω_m on v_{hh} are shown in Figure 2, which are degenerate, i.e., a larger value of either would lead to a larger magnitude of v_{hh} . A larger H_0

² We take the mean of upper and lower one sigma, which is fair as the differences between them are small.

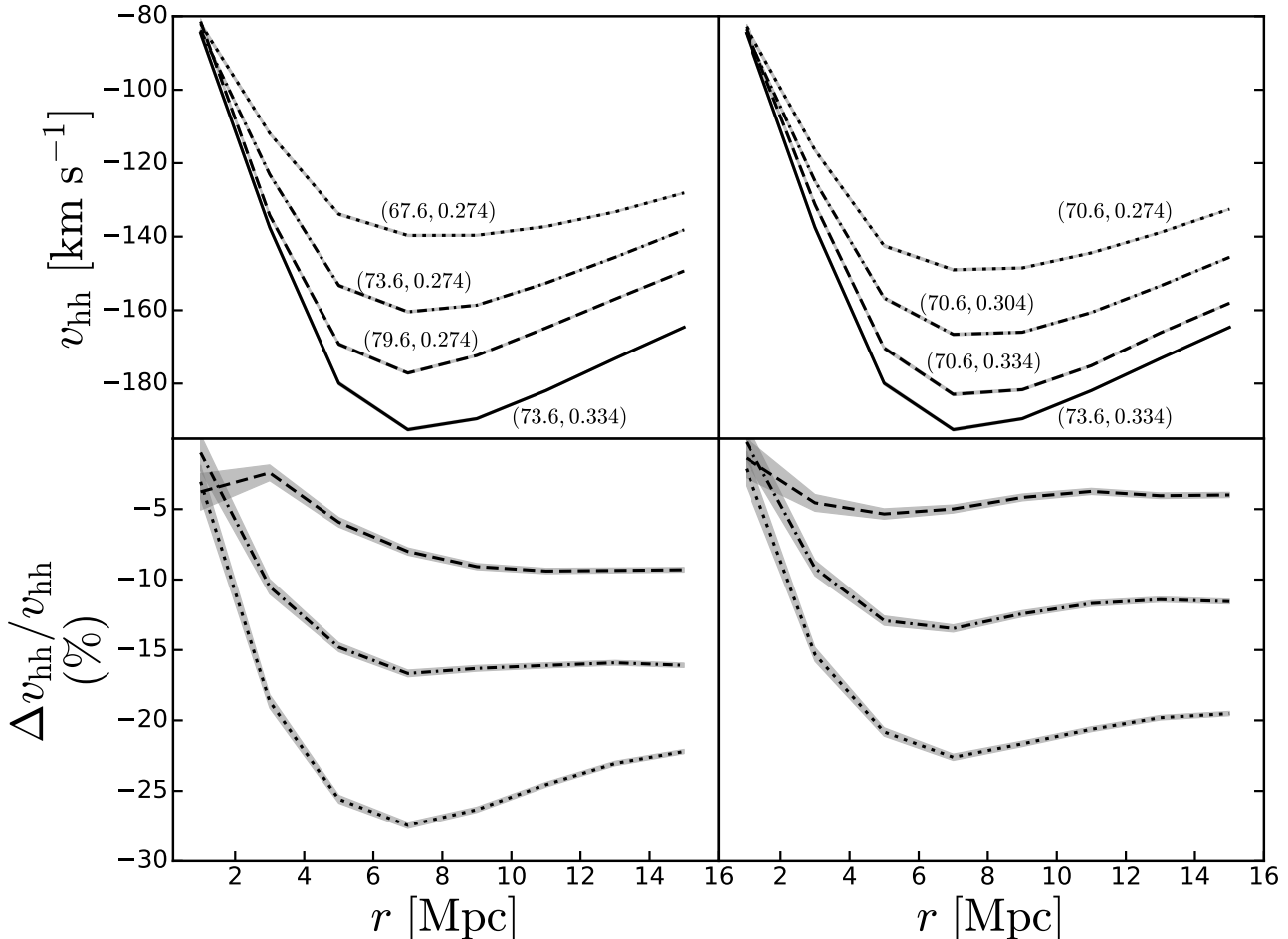


Figure 2. Halo-halo pairwise velocity v_{hh} for $\Omega_m = 0.274$ and $H_0 = 67.6$ (dotted), 73.6 (dot-dashed), and 79.6 (dashed) (left panels), as well as $H_0 = 70.6$ and $\Omega_m = 0.274$ (dotted), 0.304 (dot-dashed), and 0.334 (dashed) (right panels). The legends are for (H_0, Ω_m) , where H_0 is in $\text{km s}^{-1} \text{Mpc}^{-1}$. The fiducial case ($H_0 = 73.6$ and $\Omega_m = 0.334$) is shown as solid lines in the top row. The bottom row shows the percentage deviations between the various styled lines and the fiducial case.

with a fixed Ω_m means a higher matter density ($\Omega_m h^2$) and larger gravity, resulting in a larger magnitude of v_{hh} . Similarly, increasing Ω_m while fixing H_0 would lead to not only a higher matter density but also a smaller dark energy density (assuming a flat universe), which in turn makes v_{hh} more negative. In particular, at $r \lesssim 4$ Mpc, their impact on v_{hh} diminishes due to the reduced cosmological effects within the halo merger range.

We can apply the linear regression on the halo-halo pairwise velocity v_{hh} for each r bin,

$$v_{\text{hh}}(H_0, \Omega_m, r) = v_{\text{hh}}(73.6, 0.334, r) \times \left[C_H(r) \frac{H_0 - 73.6}{73.6} + C_m(r) \frac{\Omega_m - 0.334}{0.334} + 1 \right], \quad (12)$$

where $C_H(r)$ and $C_m(r)$ are the r -dependent fitting parameters. Here, H_0 is in units of $\text{km s}^{-1} \text{Mpc}^{-1}$. To evaluate the impacts of cosmic variance from cosmological simulations, we analyze v_{hh} across various H_0 and Ω_m using two different initial realizations. We find that although the cosmic variance causes notable changes in

v_{hh} values for the same set of H_0 and Ω_m between two realizations, the effects of H_0 and Ω_m on v_{hh} remain consistent between different initial realizations within the relevant range. Therefore, one realization is adequate for extracting $C_H(r)$ and $C_m(r)$ in Eq. (12). To reduce the impact of cosmic variance on the values of $v_{\text{hh}}(73.6, 0.334, r)$, we replace $v_{\text{hh}}(73.6, 0.334, r)$ by its mean of a total of 12 simulations mentioned in Section 2, $\bar{v}_{\text{hh}}(73.6, 0.334, r)$. More details are provided in Appendix B.

Then, a χ^2 is defined as

$$\chi^2(H_0, \Omega_m) = \sum_{ij} D_v(H_0, \Omega_m, r_i) C_{ij}^{-1} D_v(H_0, \Omega_m, r_j), \quad (13)$$

where $D_v(H_0, \Omega_m, r_i) \equiv v_{\text{gg}}(H_0, \Omega_m, r_i) - v_{\text{hh}}(H_0, \Omega_m, r_i)$. The covariance matrix $C_{ij} = [C_{\text{gg}}]_{ij} + (\Delta \bar{v}_{\text{hh}})^2 \delta_{ij}$, where $\Delta \bar{v}_{\text{hh}}$ is the uncertainty of the simulation model in the corresponding r bin, which originates from the uncertainties of fitting parameters C_m and C_H in Eq. (12).

The calculations for the observational matrix C_{gg} are discussed in Section 3.5.

We assume the likelihood function follows the Gaussian form

$$\mathcal{L}(H_0, \Omega_m) \sim e^{-\chi^2(H_0, \Omega_m)/2} p(H_0) p(\Omega_m), \quad (14)$$

where $p(H_0)$ and $p(\Omega_m)$ are the uniform priors for H_0 and Ω_m , with ranges $[60, 80] \text{ km s}^{-1} \text{ Mpc}^{-1}$ and $[0.2, 0.4]$, respectively.

We use the Markov Chain Monte Carlo (MCMC) method to apply the fitting, which is employed by `emcee` (Foreman-Mackey et al. 2013). At each step, given (H_0, Ω_m) , v_{hh} is calculated using Eq. (12), while v_p and positions of galaxies are recalculated by Eqs. (6) and (9), respectively. Then, v_{gg} is calculated by Eq. (10). With the knowledge of v_{hh} and v_{gg} , we calculate the likelihood \mathcal{L} by Eq. (14).

Our MCMC results are shown in the left panel of Figure 3, and the mean values with 68% confidence level (CL) are $H_0 = 75.5 \pm 1.4 \text{ km s}^{-1} \text{ Mpc}^{-1}$ and $\Omega_m = 0.311_{-0.028}^{+0.029}$, which are consistent with the SH0ES result ($H_0 = 73.04 \pm 1.04 \text{ km s}^{-1} \text{ Mpc}^{-1}$, Riess et al. 2022) and both Planck ($\Omega_m = 0.3153 \pm 0.0073$, Planck Collaboration et al. 2020) and Pantheon+ results ($\Omega_m = 0.334 \pm 0.018$, Brout et al. 2022), respectively. The current uncertainty on H_0 (Ω_m) is 2% (9%). The right panel of Figure 3 shows v_{hh} (from simulation) and v_{gg} (from observation) at the mean values of H_0 and Ω_m .

Moreover, we can also estimate the precision we can achieve if the Jackknife and peculiar velocity errors are negligible, as discussed in Section 3.5. Then, the projected uncertainties would be $(+0.43, -0.42) \text{ km s}^{-1} \text{ Mpc}^{-1}$ for H_0 and $(+0.0073, -0.0074)$ for Ω_m , or 0.6% and 2%, respectively.

A. TESTS ON THE CHOICE OF v_p^{max}

We estimate the line-of-sight peculiar velocity v_p of a galaxy using the halo catalog from the `Uchuu` simulation (Ishiyama et al. 2021), selecting host halos within the same virial mass range $[10^{11}, 10^{13}] M_{\odot}$ as described in the main text, obtaining a total of 223,900,197 host halos. We randomly generate three observers inside the `Uchuu` simulation box and calculate the corresponding v_p of the host halos. The v_p histograms follow Gaussian distributions with $3\sigma = 960.5, 963.2, 960.3 \text{ km s}^{-1}$, respectively. Based on this, taking $H_0 = 74.6 \text{ km s}^{-1} \text{ Mpc}^{-1}$

³ Here, “mean” is the arithmetic average of all pairs of galaxies with the same separations r .

5. CONCLUSIONS

In this Letter, we measure H_0 and Ω_m using the mean galaxy pairwise peculiar velocity³ in the nonlinear and quasi-linear region for the first time. By applying MCMC to fit simulation models with the galaxy data drawn from the CF-4 grouped catalog, we find that

(i) we can achieve 2% and 9% measurements in H_0 and Ω_m , respectively, and obtain $H_0 = 75.5 \pm 1.4 \text{ km s}^{-1} \text{ Mpc}^{-1}$ and $\Omega_m = 0.311_{-0.028}^{+0.029}$ with 68% CL. The value of H_0 we obtain is consistent with the SH0ES result (Riess et al. 2022), and our Ω_m agrees with both the Planck (Planck Collaboration et al. 2020) and Pantheon+ results (Brout et al. 2022);

(ii) if, in the future, the statistical errors become negligible, we can get much more precise measurements of H_0 and Ω_m , with 0.6% and 2% uncertainty, respectively.

We thank Renbin Yan, Yin-Zhe Ma, and R. Brent Tully for discussions, and the anonymous referee for helpful comments. The computational resources used for the simulations in this work were kindly provided by the Chinese University of Hong Kong Central Research Computing Cluster. This research is supported by grants from the Research Grants Council of the Hong Kong Special Administrative Region, China, under Project No.s AoE/P-404/18 and 14300223. S.L. acknowledges the support by the National Natural Science Foundation of China (NSFC) grant (no. 12473015). H.H. is supported by the China Postdoctoral Science Foundation grant No. 2024M763213. All plots in this Letter are generated by `Matplotlib` (Hunter 2007) and `Getdist` (Lewis 2019), together with `SciPy` (Virtanen et al. 2020), `NumPy` (Harris et al. 2020).

APPENDIX

and $\Omega_m = 0.27$ ⁴ as suggested by CF-4 (Tully et al. 2023), we apply a bound on the peculiar velocity calculated from Eq. (6), $|v_p| \leq v_p^{\text{max}}$, with $v_p^{\text{max}} = 1000 \text{ km s}^{-1}$. This leaves us with 10,014 galaxies, which we analyze in the main text.

Then, we examine how the choice of v_p^{max} affects v_{gg} by adjusting v_p^{max} around 1000 km s^{-1} . We sample 15 linear bins within $r \in [0, 30] \text{ Mpc}$, calculating v_{gg} for $v_p^{\text{max}} = 800, 1000, \text{ and } 1200 \text{ km s}^{-1}$. The results are shown in the upper subpanel of Figure 4, while the lower subpanel presents the deviation of v_{gg} for different v_p^{max} values from that for $v_p^{\text{max}} = 1000 \text{ km s}^{-1}$, quantified as

⁴ Although Ω_m differs from our final MCMC results, we have confirmed that our results remain practically unchanged for the values of Ω_m between 0.27 and 0.32.

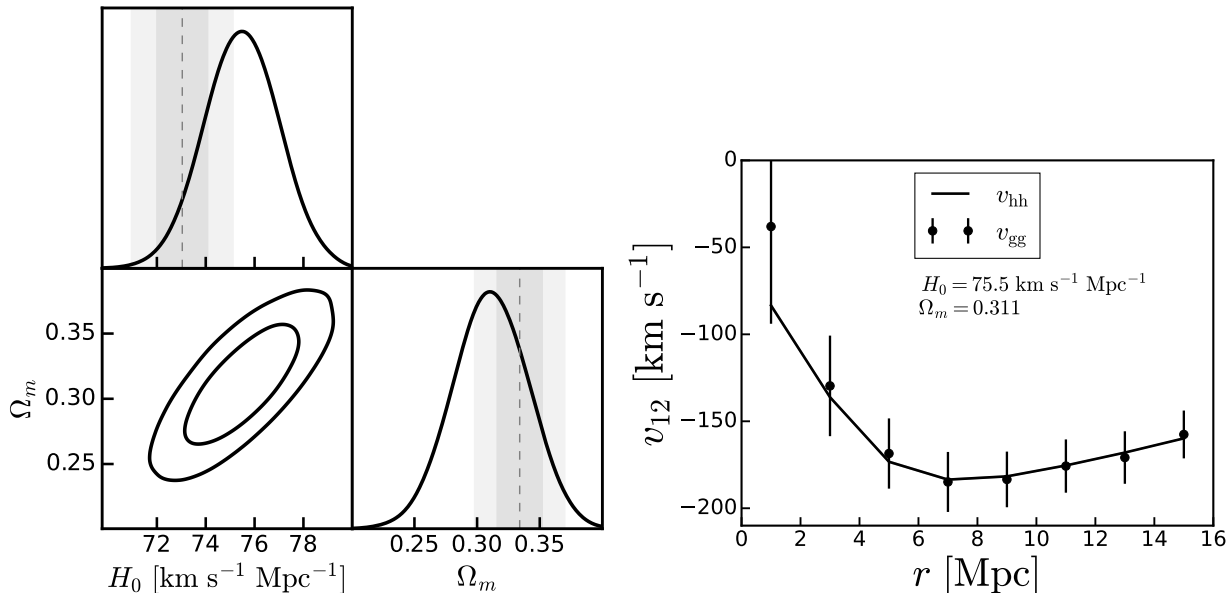


Figure 3. Contours (at 68% and 95% CL) and PDFs for H_0 and Ω_m (left panel). The gray bands in H_0 and Ω_m PDFs are from SH0ES ($H_0 = 73.04 \pm 1.04 \text{ km s}^{-1} \text{Mpc}^{-1}$, Riess et al. 2022) and Pantheon+ ($\Omega_m = 0.334 \pm 0.018$, Brout et al. 2022), respectively. Halo-halo pairwise velocity v_{hh} (solid line, from simulation) and galaxy-galaxy pairwise velocity v_{gg} (data points with error bars, from observation) when taking H_0 and Ω_m at the mean values of the MCMC results are shown in the right panel.

the number of sigmas, assuming Gaussian distributions,

$$n_\sigma(r) \equiv \frac{v_{\text{gg}}(r)|_{v_{p,1}^{\text{max}}} - v_{\text{gg}}(r)|_{v_{p,0}^{\text{max}}}}{\sqrt{\Delta v_{\text{gg}}^2(r)|_{v_{p,1}^{\text{max}}} + \Delta v_{\text{gg}}^2(r)|_{v_{p,0}^{\text{max}}}}}, \quad (\text{A1})$$

where $v_{p,1}^{\text{max}} = 800$ or 1200 km s^{-1} , while $v_{p,0}^{\text{max}} = 1000 \text{ km s}^{-1}$. The error of v_{gg} , denoted as Δv_{gg} , is evaluated as per Section 3.5. We find that v_{gg} is not sensitive to the exact value of v_p^{max} for $r \lesssim 16 \text{ Mpc}$, i.e., $|n_\sigma| \lesssim 1$.

Consequently, throughout this Letter, we calculate v_{hh} and v_{gg} using 8 linear bins within $r \in [0, 16] \text{ Mpc}$. We also check the effects of binning numbers, by repeating the analysis in the main text using 4 and 12 linear bins within this range and find that the constraints on H_0 and Ω_m are not affected.

B. COSMIC VARIANCE

In Figure 5, we show v_{hh} for various (H_0, Ω_m) combinations derived from two distinct initial realizations (solid and dashed lines). While the values of v_{hh} exhibit significant variations between realizations due to the cosmic variance (upper panel of Figure 5), the effects of H_0 and Ω_m , expressed as changes of halo-halo pairwise velocity v_{hh} relative to the fiducial case (Eq. (12)), remain consistent across different initial seeds (lower panel of Figure 5).

Consequently, in the main text, we only use one random seed to estimate the effects of H_0 and Ω_m , and we average 12 simulations for the fiducial case ($H_0 = 73.6 \text{ km s}^{-1} \text{Mpc}^{-1}$ and $\Omega_m = 0.334$) to reduce the effects of cosmic variance.

REFERENCES

- Abdalla, E., Abellán, G. F., Aboubrahim, A., et al. 2022, *Journal of High Energy Astrophysics*, 34, 49, doi: [10.1016/j.jheap.2022.04.002](https://doi.org/10.1016/j.jheap.2022.04.002)
- Anand, G. S., Tully, R. B., Rizzi, L., Riess, A. G., & Yuan, W. 2022, *ApJ*, 932, 15, doi: [10.3847/1538-4357/ac68df](https://doi.org/10.3847/1538-4357/ac68df)
- Angulo, R. E., & Pontzen, A. 2016, *MNRAS*, 462, L1, doi: [10.1093/mnras/slw098](https://doi.org/10.1093/mnras/slw098)
- Astropy Collaboration, Robitaille, T. P., Tollerud, E. J., et al. 2013, *A&A*, 558, A33, doi: [10.1051/0004-6361/201322068](https://doi.org/10.1051/0004-6361/201322068)
- Astropy Collaboration, Price-Whelan, A. M., Sipőcz, B. M., et al. 2018, *AJ*, 156, 123, doi: [10.3847/1538-3881/aabc4f](https://doi.org/10.3847/1538-3881/aabc4f)
- Astropy Collaboration, Price-Whelan, A. M., Lim, P. L., et al. 2022, *ApJ*, 935, 167, doi: [10.3847/1538-4357/ac7c74](https://doi.org/10.3847/1538-4357/ac7c74)
- Behroozi, P. S., Wechsler, R. H., & Wu, H.-Y. 2013, *ApJ*, 762, 109, doi: [10.1088/0004-637X/762/2/109](https://doi.org/10.1088/0004-637X/762/2/109)
- Bell, E. F., McIntosh, D. H., Katz, N., & Weinberg, M. D. 2003, *ApJS*, 149, 289, doi: [10.1086/378847](https://doi.org/10.1086/378847)
- Bhattacharya, S., & Kosowsky, A. 2007, *ApJL*, 659, L83, doi: [10.1086/517523](https://doi.org/10.1086/517523)

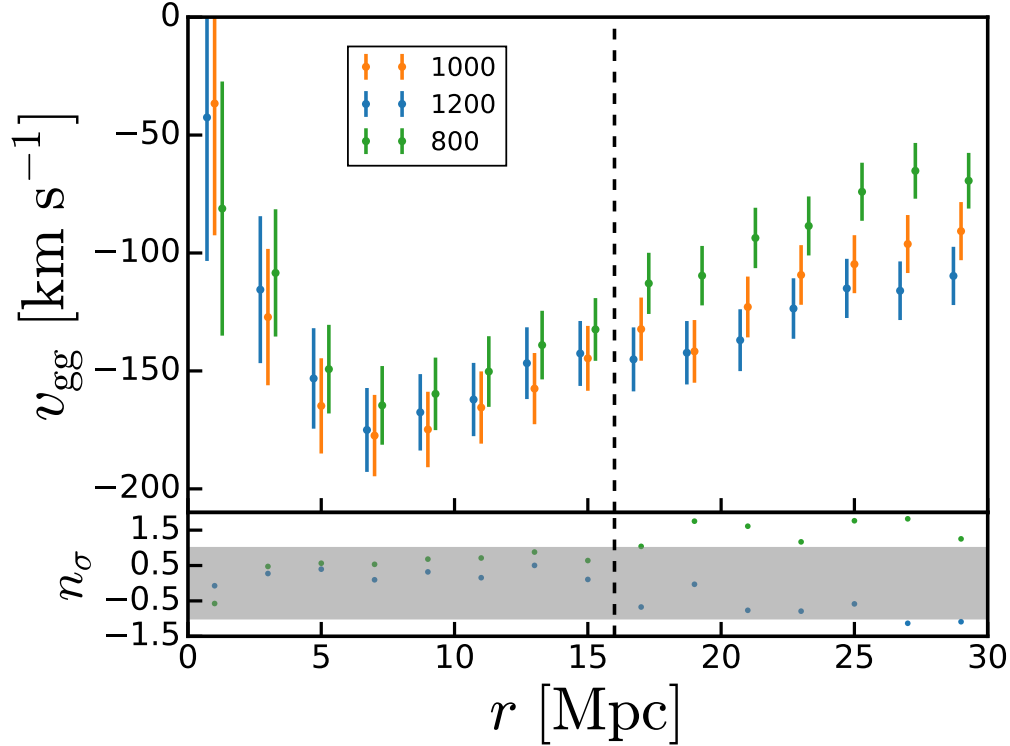


Figure 4. Galaxy-galaxy pairwise velocity for various v_p^{\max} (in km s^{-1}) represented by different colors, with both statistical and systematic error bars (upper subpanel). For clarity, the identical r bins depicted in different colors are shifted horizontally slightly. The lower subpanel shows the deviations of $v_p^{\max} = 800$ and 1200 km s^{-1} cases from $v_p^{\max} = 1000$ km s^{-1} , quantified in sigma units (n_σ). The gray band denotes $\pm 1\sigma$ deviation. The black dashed line indicates $r = 16$ Mpc.

- . 2008, *PhRvD*, 77, 083004,
doi: [10.1103/PhysRevD.77.083004](https://doi.org/10.1103/PhysRevD.77.083004)
- Bhattacharya, S., Kosowsky, A., Newman, J. A., & Zentner, A. R. 2011, *PhRvD*, 83, 043004,
doi: [10.1103/PhysRevD.83.043004](https://doi.org/10.1103/PhysRevD.83.043004)
- Bibiano, A., & Croton, D. J. 2017, *MNRAS*, 467, 1386,
doi: [10.1093/mnras/stx070](https://doi.org/10.1093/mnras/stx070)
- Birrer, S., Shajib, A. J., Galan, A., et al. 2020, *A&A*, 643, A165, doi: [10.1051/0004-6361/202038861](https://doi.org/10.1051/0004-6361/202038861)
- Blakeslee, J. P., Jensen, J. B., Ma, C.-P., Milne, P. A., & Greene, J. E. 2021, *ApJ*, 911, 65,
doi: [10.3847/1538-4357/abe86a](https://doi.org/10.3847/1538-4357/abe86a)
- Brout, D., Scolnic, D., Popovic, B., et al. 2022, *ApJ*, 938, 110, doi: [10.3847/1538-4357/ac8e04](https://doi.org/10.3847/1538-4357/ac8e04)
- Bryan, G. L., & Norman, M. L. 1998, *ApJ*, 495, 80,
doi: [10.1086/305262](https://doi.org/10.1086/305262)
- Calafut, V., Gallardo, P. A., Vavagiakis, E. M., et al. 2021, *PhRvD*, 104, 043502, doi: [10.1103/PhysRevD.104.043502](https://doi.org/10.1103/PhysRevD.104.043502)
- Choi, S. K., Hasselfield, M., Ho, S.-P. P., et al. 2020, *JCAP*, 2020, 045, doi: [10.1088/1475-7516/2020/12/045](https://doi.org/10.1088/1475-7516/2020/12/045)
- Crocce, M., Pueblas, S., & Scoccimarro, R. 2006, *MNRAS*, 373, 369, doi: [10.1111/j.1365-2966.2006.11040.x](https://doi.org/10.1111/j.1365-2966.2006.11040.x)
- Davis, T. M., & Scrimgeour, M. I. 2014, *MNRAS*, 442, 1117, doi: [10.1093/mnras/stu920](https://doi.org/10.1093/mnras/stu920)
- Dupuy, A., Courtois, H. M., & Kubik, B. 2019, *MNRAS*, 486, 440, doi: [10.1093/mnras/stz901](https://doi.org/10.1093/mnras/stz901)
- Feldman, H., Juszkievicz, R., Ferreira, P., et al. 2003, *ApJL*, 596, L131, doi: [10.1086/379221](https://doi.org/10.1086/379221)
- Ferreira, P. G., Juszkievicz, R., Feldman, H. A., Davis, M., & Jaffe, A. H. 1999, *ApJL*, 515, L1, doi: [10.1086/311959](https://doi.org/10.1086/311959)
- Foreman-Mackey, D., Hogg, D. W., Lang, D., & Goodman, J. 2013, *PASP*, 125, 306, doi: [10.1086/670067](https://doi.org/10.1086/670067)
- Freedman, W. L. 2021, *ApJ*, 919, 16,
doi: [10.3847/1538-4357/ac0e95](https://doi.org/10.3847/1538-4357/ac0e95)
- Gayathri, V., Healy, J., Lange, J., et al. 2021, *ApJL*, 908, L34, doi: [10.3847/2041-8213/abe388](https://doi.org/10.3847/2041-8213/abe388)
- Harris, C. R., Millman, K. J., van der Walt, S. J., et al. 2020, *Nature*, 585, 357, doi: [10.1038/s41586-020-2649-2](https://doi.org/10.1038/s41586-020-2649-2)
- Howlett, C., Staveley-Smith, L., Elahi, P. J., et al. 2017, *MNRAS*, 471, 3135, doi: [10.1093/mnras/stx1521](https://doi.org/10.1093/mnras/stx1521)
- Huang, C. D., Riess, A. G., Yuan, W., et al. 2020, *ApJ*, 889, 5, doi: [10.3847/1538-4357/ab5dbd](https://doi.org/10.3847/1538-4357/ab5dbd)
- Hunter, J. D. 2007, *Computing in Science and Engineering*, 9, 90, doi: [10.1109/MCSE.2007.55](https://doi.org/10.1109/MCSE.2007.55)

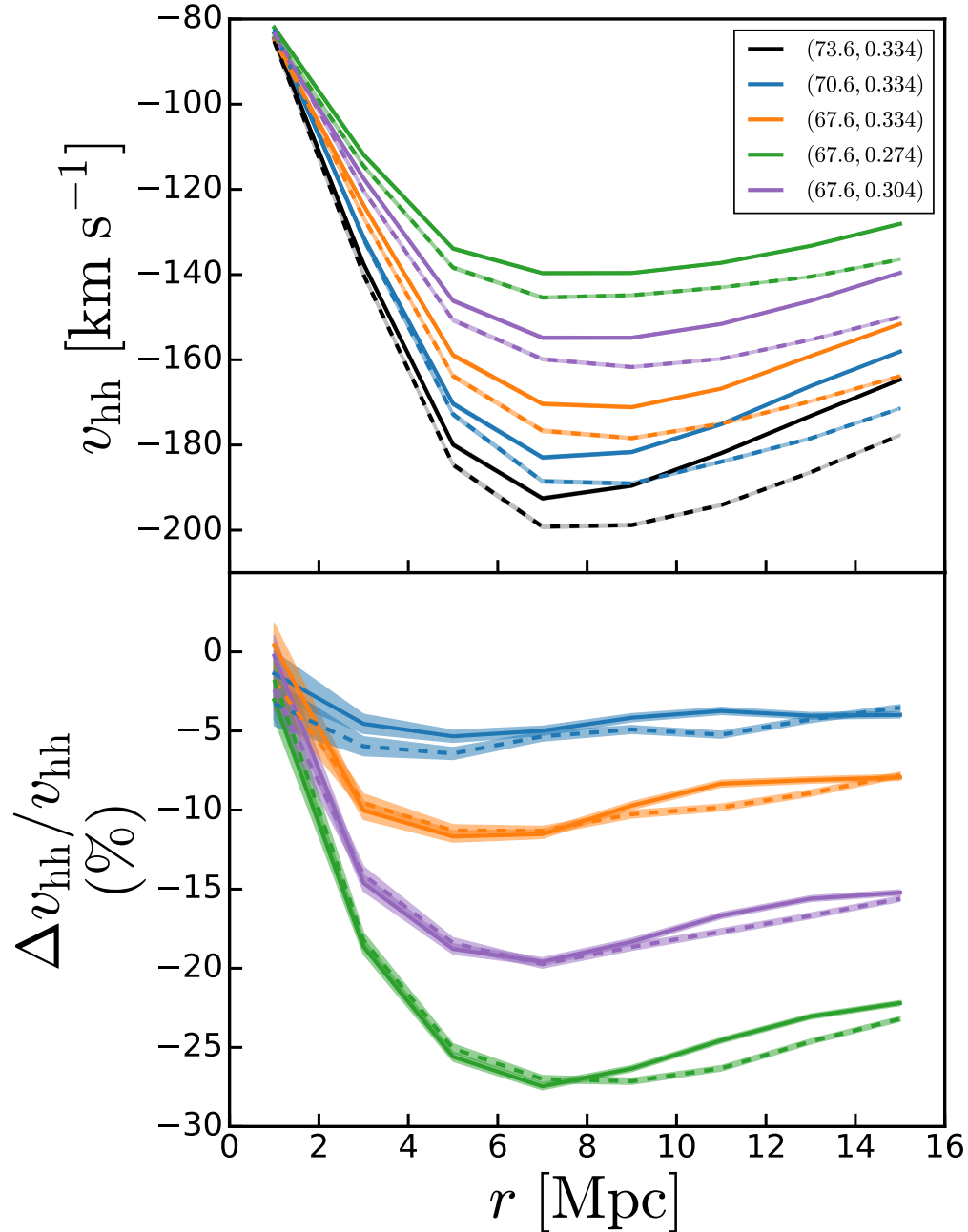


Figure 5. Halo-halo pairwise velocity (v_{hh} , upper panel) and percentage deviations of halo-halo pairwise velocity with respect to the fiducial case ($H_0 = 73.6$ and $\Omega_m = 0.334$) (lower panel), for two different initial random seeds (solid and dashed lines). The shaded bands indicate the 1σ statistical error. The legends are for (H_0, Ω_m) , where H_0 is in $\text{km s}^{-1} \text{Mpc}^{-1}$.

Ishiyama, T., Prada, F., Klypin, A. A., et al. 2021, MNRAS, 506, 4210, doi: [10.1093/mnras/stab1755](https://doi.org/10.1093/mnras/stab1755)

Jaber, M., Hellwing, W. A., García-Farieta, J. E., Gupta, S., & Bilicki, M. 2024, Phys. Rev. D, 109, 123528, doi: [10.1103/PhysRevD.109.123528](https://doi.org/10.1103/PhysRevD.109.123528)

Juszkiewicz, R., Ferreira, P. G., Feldman, H. A., Jaffe, A. H., & Davis, M. 2000, Science, 287, 109, doi: [10.1126/science.287.5450.109](https://doi.org/10.1126/science.287.5450.109)

Juszkiewicz, R., Springel, V., & Durrer, R. 1999, ApJL, 518, L25, doi: [10.1086/312055](https://doi.org/10.1086/312055)

Khetan, N., Izzo, L., Branchesi, M., et al. 2021, A&A, 647, A72, doi: [10.1051/0004-6361/202039196](https://doi.org/10.1051/0004-6361/202039196)

Klypin, A., Prada, F., & Byun, J. 2020, MNRAS, 496, 3862, doi: [10.1093/mnras/staa734](https://doi.org/10.1093/mnras/staa734)

Kosowsky, A., & Bhattacharya, S. 2009, PhRvD, 80, 062003, doi: [10.1103/PhysRevD.80.062003](https://doi.org/10.1103/PhysRevD.80.062003)

- Kourkchi, E., Tully, R. B., Anand, G. S., et al. 2020, *ApJ*, 896, 3, doi: [10.3847/1538-4357/ab901c](https://doi.org/10.3847/1538-4357/ab901c)
- Lewis, A. 2019, arXiv e-prints, arXiv:1910.13970, doi: [10.48550/arXiv.1910.13970](https://doi.org/10.48550/arXiv.1910.13970)
- Lewis, A., Challinor, A., & Lasenby, A. 2000, *ApJ*, 538, 473, doi: [10.1086/309179](https://doi.org/10.1086/309179)
- Linder, E. V. 2005, *PhRvD*, 72, 043529, doi: [10.1103/PhysRevD.72.043529](https://doi.org/10.1103/PhysRevD.72.043529)
- Ma, Y.-Z., Li, M., & He, P. 2015, *A&A*, 583, A52, doi: [10.1051/0004-6361/201526051](https://doi.org/10.1051/0004-6361/201526051)
- Makarov, D., Prugniel, P., Terekhova, N., Courtois, H., & Vauglin, I. 2014, *A&A*, 570, A13, doi: [10.1051/0004-6361/201423496](https://doi.org/10.1051/0004-6361/201423496)
- Mo, H., van den Bosch, F. C., & White, S. 2010, *Galaxy Formation and Evolution* (Cambridge, UK: Cambridge University Press)
- Moresco, M., Amati, L., Amendola, L., et al. 2022, *Living Reviews in Relativity*, 25, 6
- Moster, B. P., Somerville, R. S., Maulbetsch, C., et al. 2010, *ApJ*, 710, 903, doi: [10.1088/0004-637X/710/2/903](https://doi.org/10.1088/0004-637X/710/2/903)
- Mueller, E.-M., de Bernardis, F., Bean, R., & Niemack, M. D. 2015a, *ApJ*, 808, 47, doi: [10.1088/0004-637X/808/1/47](https://doi.org/10.1088/0004-637X/808/1/47)
- . 2015b, *PhRvD*, 92, 063501, doi: [10.1103/PhysRevD.92.063501](https://doi.org/10.1103/PhysRevD.92.063501)
- Navas, S., Amsler, C., Gutsche, T., et al. 2024, *PhRvD*, 110, 030001, doi: [10.1103/PhysRevD.110.030001](https://doi.org/10.1103/PhysRevD.110.030001)
- Peebles, P. J. E. 2020, *The large-scale structure of the universe* (Princeton University Press)
- Perivolaropoulos, L., & Skara, F. 2022, *NewAR*, 95, 101659, doi: [10.1016/j.newar.2022.101659](https://doi.org/10.1016/j.newar.2022.101659)
- Pesce, D. W., Braatz, J. A., Reid, M. J., et al. 2020, *ApJL*, 891, L1, doi: [10.3847/2041-8213/ab75f0](https://doi.org/10.3847/2041-8213/ab75f0)
- Planck Collaboration, Aghanim, N., Akrami, Y., et al. 2020, *A&A*, 641, A6, doi: [10.1051/0004-6361/201833910](https://doi.org/10.1051/0004-6361/201833910)
- Riess, A. G., Yuan, W., Macri, L. M., et al. 2022, *ApJL*, 934, L7, doi: [10.3847/2041-8213/ac5c5b](https://doi.org/10.3847/2041-8213/ac5c5b)
- Schombert, J., McGaugh, S., & Lelli, F. 2020, *AJ*, 160, 71, doi: [10.3847/1538-3881/ab9d88](https://doi.org/10.3847/1538-3881/ab9d88)
- Schöneberg, N., Abellán, G. F., Sánchez, A. P., et al. 2022, *PhR*, 984, 1, doi: [10.1016/j.physrep.2022.07.001](https://doi.org/10.1016/j.physrep.2022.07.001)
- Springel, V. 2005, *MNRAS*, 364, 1105, doi: [10.1111/j.1365-2966.2005.09655.x](https://doi.org/10.1111/j.1365-2966.2005.09655.x)
- SPT-3G Collaboration, Balkenhol, L., Dutcher, D., et al. 2023, *PhRvD*, 108, 023510, doi: [10.1103/PhysRevD.108.023510](https://doi.org/10.1103/PhysRevD.108.023510)
- The Ligo Scientific Collaboration, The VIRGO Collaboration, The Kagra Collaboration, et al. 2023, *ApJ*, 949, 76, doi: [10.3847/1538-4357/ac74bb](https://doi.org/10.3847/1538-4357/ac74bb)
- Tully, R. B., Courtois, H. M., & Sorce, J. G. 2016, *AJ*, 152, 50, doi: [10.3847/0004-6256/152/2/50](https://doi.org/10.3847/0004-6256/152/2/50)
- Tully, R. B., Kourkchi, E., Courtois, H. M., et al. 2023, *ApJ*, 944, 94, doi: [10.3847/1538-4357/ac94d8](https://doi.org/10.3847/1538-4357/ac94d8)
- Virtanen, P., Gommers, R., Oliphant, T. E., et al. 2020, *Nature Methods*, 17, 261, doi: [10.1038/s41592-019-0686-2](https://doi.org/10.1038/s41592-019-0686-2)
- Willmer, C. N. A. 2018, *ApJS*, 236, 47, doi: [10.3847/1538-4365/aabfdf](https://doi.org/10.3847/1538-4365/aabfdf)
- Wong, K. C., Suyu, S. H., Chen, G. C. F., et al. 2020, *MNRAS*, 498, 1420, doi: [10.1093/mnras/stz3094](https://doi.org/10.1093/mnras/stz3094)
- Zhang, W., Chu, M.-c., Hu, R., Liao, S., & Shek, Y. 2024, *MNRAS*, 529, 360, doi: [10.1093/mnras/stae511](https://doi.org/10.1093/mnras/stae511)